Article

Effect of steel slag powder content and curing condition on the performance of alkali activated materials based ultra-high performance concrete (UHPC) matrix

Kangyi Shi [1], Hongyang Deng [1,*], Jinxuan Hu[1], Junqi Zhou[1], XinHua Cai[2], Zhiwei Liu[1]

[1] School of Civil Engineering and Architecture,Wuhan Polytechnic University,Wuhan 430072, China; shikangyisky@126.com(K.S.);hujinxuan@whpu.edu.cn(J.H.);wlmm1128@yeah.net(J.Z.);tonyliuzhiwei@whpu.edu.cn(Z.L.)

[2] State Key Laboratory of Water Resources and Hydropower Engineering Science, Wuhan University,Wuhan 430072, China;caixinhua@whu.edu.cn(X.C.)

* Correspondence: denghongyang@whpu.edu.cn

Abstract: The accumulation of steel slag and other industrial solid wastes has caused serious environmental pollution and resource waste. The resource utilization of steel slag is imminent. In this paper, alkali activated materials ultra-high performance concrete (AAM-UHPC) was prepared by replacing GGBFS powder with different proportions of steel slag powder, and its workability, mechanical properties, curing condition, microstructure, and pore structure were investigated. The results illustrate that the incorporation of steel slag powder can significantly delay the setting time and improve the flowability of AAM-UHPC, making it possible for engineering applications. The mechanical properties of AAM-UHPC showed a tendency to increase and then decrease with the increase of steel slag dosing, and reached the best performance at 30% dosage of steel slag. The maximum compressive strength and flexural strength are 157.1 MPa and 16.32 MPa, respectively. High temperature steam or hot water curing at early age was beneficial to the strength development of AAM-UHPC, but continuous high temperature hot and humid curing would lead to strength inversion. When the dosage of steel slag is 30%, the average pore diameter of the matrix is only 8.43nm, and the appropriate steel slag dosage can reduce the heat of hydration and refine the pore size distribution, making the matrix more dense.

Keywords: Ultra-high performance concrete; Steel slag powder; Alkali activated materials; Curing condition; microstructure

1. Introduction

The main characteristics of ultra-high performance concrete (UHPC) are high compactness, high strength, and high durability, which are obtained by using a low water-cement ratio and batching with reference to the particle dense packing theory in the production process [1,2]. The unit cubic cement consumption of UHPC is four times higher than that of ordinary concrete, reaching 800~ 1000 kg/m^3 [3], while each 1 t of silicate cement produced emits the same mass of CO_2 into the atmosphere [4]. The high cement consumption makes UHPC costly and also has a negative impact on the environment and the heat of hydration [5–7], so with the arrival of the carbon peak in the construction industry, more and more researchers are focusing on using new materials and technologies to reduce the cement consumption, carbon emission and energy consumption of UHPC while ensuring its excellent performance [8].

China's annual industrial solid waste is about 3.6 billion tonnes, with a historical stockpile of over 60 billion tonnes, covering an area of over 20,000 square kilometres [9]. Among them, nearly 3 billion tonnes of steel slag are not effectively used [10], and the damage to the environment cannot be ignored. Steel slag is an industrial solid waste produced during the steel making process to remove impurities from the steel. Although steel

 doi:10.20944/preprints202304.0193.v1

slag is utilized in agriculture, environmental protection and construction [11], it is utilized in less than 30% of low value-added applications [12,13] such as fillers for basic construction or asphalt mixes due to its poor water hardening activity. Alkali activated materials (AAM) typically use silica-alumina raw materials such as ground-granulated blast-furnace slag(GGBFS) [14,15] and fly ash [16,17] as precursors, and alkali water glass [18] and hydroxide [19] as activators. AAM is considered as one of the alternatives to silicate cement [20,21] because of lower energy consumption and CO_2 emission, and it can make full use of industrial solid waste and solve the environmental problems caused by solid waste dumping. Zeng Lu et al. [22] used water glass as an activator and steel slag and GGBFS as cementitious materials to produce all-solid waste aerated concrete with better performance. Wang X et al. [23] prepared environmentally friendly steel slag-based cementitious materials from industrial solid wastes such as steel slag and calcium carbide slag, and their study showed that steel slag-based all-solid waste cementitious materials with high blending of steel slag are safe for the environment.

In the preparation of ecological UHPC [24–28], there have been some reports on the use of solid waste-based admixtures such as steel slag powder, GGBFS powder and fly ash to replace part of the silicate cement, but there are few studies on the use of solid waste-based raw materials to replace all the silicate cement in the preparation of UHPC. Chen et al. [29] investigated the effect of alkaline exciter dosage on the performance of alkali activated GGBFS concrete, which reached more than 100 MPa after 28 days of curing, and the mechanical strength of the specimens was close to that of UHPC. Choi J I et al. [30] used polyethylene fibers in combination with alkali activated GGBFS to prepare ultra-high toughness concrete with a tensile strain capacity of 7.5%. Cai R et al. [31] used a variety of activators and GGBFS to produce ultra-high strength concrete with a 28 d compressive strength of 120 MPa or more.

The prerequisite for a homogeneous UHPC mix is good workability, which requires UHPC mixes with excellent flowability, cohesiveness and water retention. The setting time is also one of the important workability properties of concrete mixes, which determines the time window for mixing, transporting and placing the mixes. One of the disadvantages of applying GGBFS as a precursor in alkali activated cementitious materials is its rapid setting time [32–35], especially when mixed with more activator to obtain higher mechanical properties [36], its setting is extremely rapid, making it extremely limited in practical engineering applications [37]. You N et al. [38] found that the amount of steel slag at 50% can significantly delay the setting time of alkali activated mortar and improve the flowability.

In this study, based on the concept of "zero-waste city" and environmental sustainability, the industrial solid wastes such as steel slag and GGBFS were used as precursors .By adjusting the ratio of raw materials to optimise the particle buildup. Na_2O-$9SiO_2$ and K_2CO_3 were used as activators to improve the active reaction. The AAM-UHPC was prepared with excellent performance, and the effects of different dosages of steel slag and curing conditions on the performance of AAM-UHPC were investigated through comparative tests.

2. Materials and Methods

2.1. Raw Materials

Precursors:Steel slag(SS) powder was supplied by Huailong New Building Material Co.(Jiangsu,China). Ground granulated blast furnace slag(GGBFS) powder was S95 GGBFS powder produced by Hengle New Building Materials Co.(Zhangjiagang,China). The "semi-densified" silica fume (SF) was produced by Huashen Smart Technology Co., Ltd (Wuhan, China) with a specific surface area of 19.915 g/cm3. In order to avoid test errors caused by large particles agglomerated in the silica fume, it was screened with a 0.015 mm square hole sieve before use.The chemical compositions of both precursors SS and GGBFS used in this research are provided below (Table 1).

Preprints (www.preprints.org) | NOT PEER-REVIEWED | Posted: 11 April 2023 doi:10.20944/preprints202304.0193.v1

Na_2O-$9SiO_2$ and K_2CO_3 of analytical grade were adopted to prepare the alkaline activator solutions. Quartz sand with particle sizes ranging from 0 to 0.5 mm, 0.5 to 1 mm, and 1 to 2 mm was selected as fine aggregate, with a mass ratio of 1:1.75:2.25 and a ratio of 1.2 for the sand and cementious material.

Table 1. Chemical compositions (wt.%)and loss on ignition (LOI)of the precursors.

	CaO	SiO_2	Al_2O_3	MgO	Fe_2O_3	MnO	P_2O_5	TiO_2	f-CaO	LOI
Steel Slag	33.26	14.52	2.9	5.68	26.53	4.35	2.41	-	-	10.62
GGBFS	37.41	30.92	15.74	8.72	0.3	-	-	2.15	0.04	4.72
Silica Fume	0.38	97.51	0.16	0.88	-	-	0.25	-	-	0.98

2.2. Mix proportions and specimens preparations

In order to study the effects of steel slag admixture and curing condition on the performance of AAM-UHPC, the mixing ratio design was optimized according to the modified Andreasen & Andersen (MA&A) model. First, the target curve was determined according to the MA&A model as shown in Equation (1), and then the particle size distribution curve was made close to the target curve by adjusting the proportion of each cementitious material, and the detailed mixture proportions are provided in Table 2.

AAM-UHPC is prepared by first dissolving Na_2O-$9SiO_2$ and K_2CO_3 in water, while mixing the cementitious material and quartz sand well, then adding the liquid phase slowly into the solid mixture, followed by slow stirring for 90 s and continuely fast stirring quickly for 60 s to make AAM-UHPC matrix, finally demolding after 24 h.

$$P\ （D）= \frac{D^q - D^q_{\min}}{D^q_{\max} - D^q_{\min}} \quad (1)$$

Where D signifies the particle size (μm); $P(D)$ represents the percentage content of particles with particle size less than D; $Dmax$ represents the maximum particle size (μm); $Dmin$ represents the minimum particle size (μm); q indicates the distribution modulus, which is taken as 0.23 [39].

Table 2. Mixture proportions (wt.%) of AAM-UHPC(mass fraction)

Group	Steel slag	GGBFS	Silica fume	Water	Activator		Curing condition
					$Na_2O·9SiO_2$	$K2CO_3$	
SS0	0	90	10	0.23	9.5	6.7	Steam
SS10	10	80					
SS30	30	60					
SS50	50	40					
SS70	70	20					
SS30-Sd	30	60					Standard
SS30-HW	30	60					Hot water

2.3. Curing Condition

A total of three types of maintenance methods were used in this study. Standard curing consisted of placing the specimens in a constant temperature and humidity maintenance chamber with the temperature set at 20 ± 1 °C and relative humidity ≥ 90% until the corresponding test age.

Steam curing was performed in an accelerated concrete curing chamber by placing the specimens in the upper steam layer of the curing chamber without touching the lower

 doi:10.20944/preprints202304.0193.v1

water storage layer, and the heating rate was set at 10 ℃/h until it reached 60 ℃, and the cooling rate was set at 15 ℃/h until it dropped to room temperature. In this study, the steam curing was continued for 3 d and 7 d. At the end of 7 d, the specimens were taken out and put into the standard curing box to continue the standard curing for 28 d. The hot water curing was performed by placing the specimens in the water storage layer at the bottom of the accelerated concrete curing chamber, and the temperature rise and fall rate was the same as that of the steam curing.

2.4. Testing Methods

The setting time was determined using a Vicat apparatus with reference to the "Test Method for Water Consumption, Setting Time and Settlement of Cement Standard Consistency" (GB/T 1346-2011). Since the setting time of activated cementitious materials is fast, one test was conducted immediately after the slurry was poured into the metal mold, followed by tests at 2 min intervals and then at 1 min intervals.

A jump table was used to measure the flow of AAM-UHPC according to the "Method for Determination of Cementitious Sand Flow" (GB/T 2419-2005).

The compressive strength test was conducted according to the Standard Test Method for Compressive Strength of Cement Mortar (ASTM C109-12), and the specimens prepared for the compressive strength test were 50 mm×50 mm×50 mm. The flexural strength test of the specimens was conducted according to the Test Method for Strength of Cement Mortar (ISO Method) (GB/T 17671-1999), and the specimens were 40 mm×40 mm×160 mm. The average value of 3 specimens in each group was taken as the final test value.

XRD analysis of the powder samples was performed using a D8 Advance (Bruker) X-ray diffractometer with a scanning angle range of 5-70°, counting time 120s.

Gemini SEM 300 (ZEISS) scanning electron microscope was used for the microscopic analysis of the specimens, and core samples were taken from 7 groups of specimens cured for 3 d. The pore structure was tested using a V9620 (Micromeritics) high performance mercury piezometer with a maximum feed force of 60,000 psi. All specimens were dried in an oven at 60 °C for 8 h prior to testing.

3. Results and Discussion

3.1. Influence of Steel Slag Powder Dosage on workability

Figure 1a shows the effect of steel slag powder dosage on the setting time of AAM net slurry. The results indicate that the setting time of AAM net slurry gradually increases with the increase of steel slag powder dosage. The main reason is that steel slag powder, as a relatively more inert powder particle than GGBFS powder, reacts much less than GGBFS powder in the early stage, and reduces the production of reaction products[40], which can delay the setting of the slurry. From SS0 group to SS10 group, the initial and final setting time increased by 10.5% and 10.7%, respectively, when the dosage of steel slag was increased to 10%; while from SS50 group to SS70 group, the initial and final setting time only increased by 13% and 6% respectively when the amount of steel slag increased by 20%. In the case of less steel slag powder dosage, the continued addition of steel slag powder, the contribution to delay the slurry coagulation is more outstanding.

The flowability of different steel slag dosages is shown in Figure 1b. The results showed a positive relationship between the steel slag dosage and the flowability of AAM-UHPC. The adsorption of different materials to water is different [41], the water requirement of steel slag powder is less than that of GGBFS powder [42–44]. As the amount of steel slag powder increases, the mass proportion of GGBFS powder also decreases, the free water in the liquid phase relatively increases [**Error! Reference source not found.**], the C-S-H gel generated in the slurry in the short term also decreases, and at the same time the viscosity decreases, the flowability of the mix is improved .

Preprints (www.preprints.org) | NOT PEER-REVIEWED | Posted: 11 April 2023 doi:10.20944/preprints202304.0193.v1

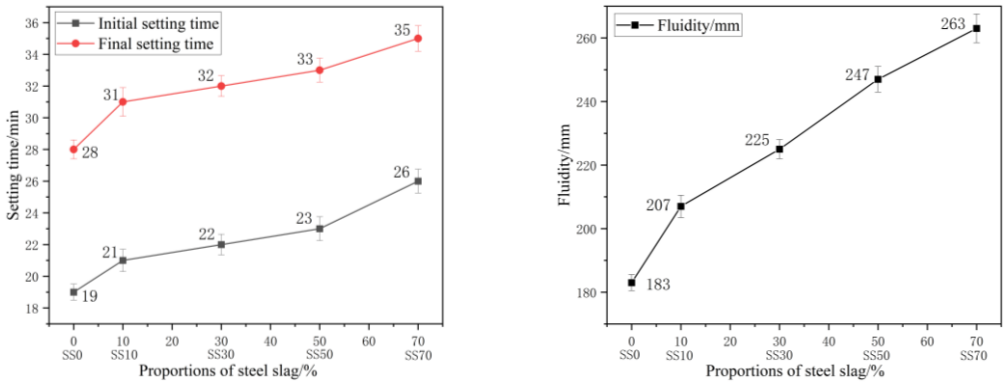

(**a**) (**b**)

Figure 1. Effect of different steel slag dosage on the workability of AAM-UHPC: (**a**) Setting time of different steel slag dosage; (**b**) Fluidity of different steel slag dosage.

3.2. Influence of steel slag powder on mechanical properties

Figure 2 shows the compressive and flexural strength of AAM-UHPC prepared with different steel slag dosages for 3d, 7d and 28d. The results showed that the 28 d compressive strength of AAM-UHPC showed a pattern of increasing and then decreasing with the increase of steel slag dosage. In terms of later strength, at 28 d, the compressive and flexural strengths of SS30 group were the highest, reaching 156.1 MPa and 15.08 MPa, respectively. From Figure 2a, compared with SS0 group without steel slag, it can be found that the compressive strength of SS30 group increased by 14.8%, reaching 156.1 MPa.

The early strength and late strength of the concrete were improved by the binary composite excitation of steel slag powder and GGBFS powder. At the same time, the incorporation of steel slag can significantly improve the workability, which shows a good composite superposition effect [46]. The compressive strength of SS30 group is 12.7% higher than that of SS70 group with a high amount of steel slag, and the excessive amount of steel slag leads to the relative reduction of active components in the system, which in turn leads to the decrease of mechanical properties.

From Figure 2b,it can be found that the flexural strength of AAM-UHPC first increases and then decreases with the increase of steel slag dosage, reaching 16.45 MPa in SS30 group. The flexural strength of SS0 group at 28d decreased by 37.14% compared with that at 3 d, while that of SS30 group decreased by only 0.7%, while that of SS70 group increased by 2.6%.It can be concluded that although the active components in the early steam curing are almost depleted in the reaction, but the better crystallized C_2S and other minerals in the steel slag powder will continue to hydrate at a later stage, and the generated hydration products fill the pores and provide a guarantee for the growth of mechanical properties at a later stage, and the degree of inversion of flexural strength gradually decreases with the increase of steel slag admixture.

At each age, the compressive and flexural strengths of the SS10 group and SS30 group met the criteria of RPC100 grade in the specification "Reactive Powder Concrete" (GB/T 31387-2015). Based on the workability and mechanical properties of each group, SS30 group was selected for the production of AAM-UHPC.

Preprints (www.preprints.org) | NOT PEER-REVIEWED | Posted: 11 April 2023 doi:10.20944/preprints202304.0193.v1

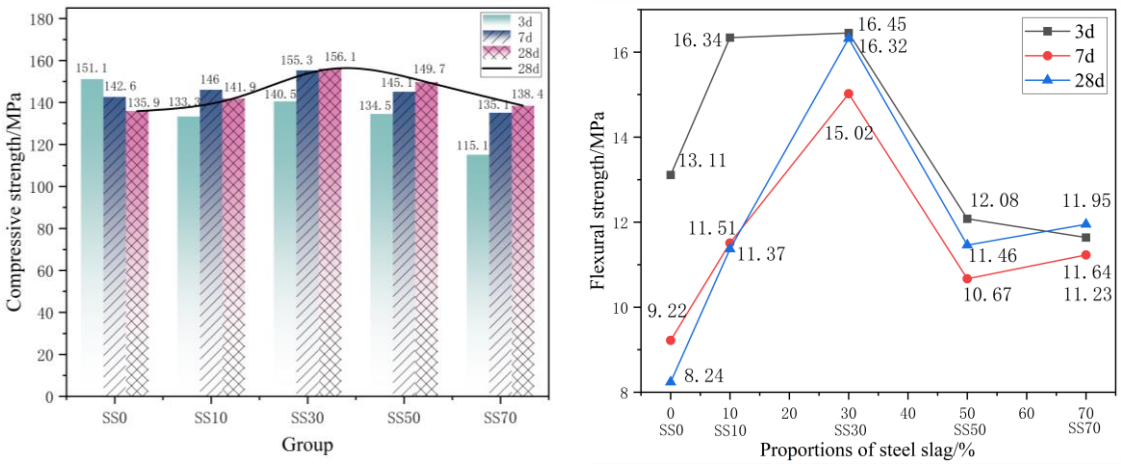

(**a**) (**b**)

Figure 2. Effect of different steel slag dosage on the mechanical properties of AAM-UHPC: (**a**) Compressive strength of steel slag with different dosage; (**b**) Flexural strength of steel slag with different dosage.

3.3. Influence of curing condition on the mechanical properties

At present, in order to maximize the use of the cementing activity of steel slag, the active activation methods commonly used in the industry include mechanical activation, chemical activation, and high-temperature activation. Studies have shown [47] that Si-O bonds and Al-O bonds in steel slag are more likely to break at high temperatures, and high temperatures are conducive to glass depolymerization, which can accelerate the reaction process of steel slag under chemical activation. Both steam and hot water curing fall into the category of high temperature activation in this paper.

The mechanical strengths of AAM-UHPC at 3 d, 7 d, and 28 d under different curing conditions are shown in Figure 3. The results showed that the 3 d steam and hot water curing significantly improved the mechanical properties significantly, but the long-term hot and humid curing was detrimental to the mechanical property development of AAM-UHPC. The compressive strengths at 3 d for steam and hot water curing were 46.2% and 42.6% higher than those in the standard curing case, respectively. The compressive strength of the steam-cured specimens at 7 d was 8.2% higher than that at 3 d, while that of the hot water-cured specimens was 10.8% lower. Such a reverse shrinkage of mechanical properties was also observed in the flexural strength of the steam cured specimens at 7 d, which was reduced by 8.7%, but the mechanical properties recovered with subsequent standard curing up to 28 d.

From Figure 3, it can be seen that the late strength increase of steam cured specimens is extremely small, and this phenomenon is consistent with that of high-strength silicate cement concrete. The reason is that the early high temperature makes the reaction proceed rapidly, and the hydration products are extremely dense, so it is difficult for pore water to penetrate from the surface of the specimen to the internal unhydrated particles, the late hydration conditions are obstructed leading to a serious internal water shortage, which will produce a large self-drying shrinkage, resulting in internal stresses and affect the late strength growth of concrete [48,49].

The reason for the increase in mechanical strength of AAM-UHPC at the age of 28 d under three curing conditions in this paper is that the C_2S in the steel slag continues to hydrate at a later stage, and the resulting gel continues to fill the matrix pores to ensure the strength development. Comparing the different curing conditions, AAM-UHPC is suitable for the curing condition of steam curing for 3 d in the first stage and standard curing up to 28 d in the later stage.

Preprints (www.preprints.org) | NOT PEER-REVIEWED | Posted: 11 April 2023 doi:10.20944/preprints202304.0193.v1

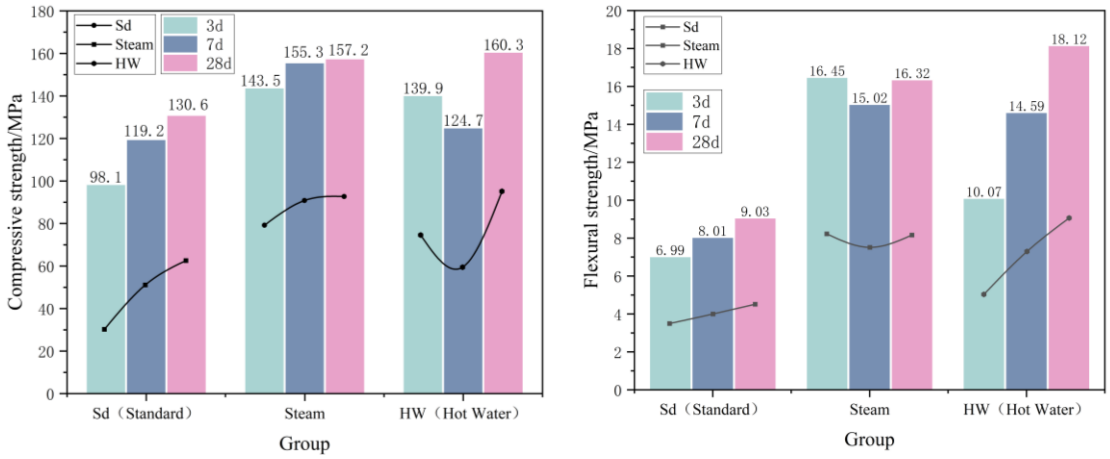

(**a**) (**b**)

Figure 3. Effect of different curing conditions on the mechanical properties of AAM-UHPC: (**a**) Compressive strength of different curing conditions(Group SS30); (**b**) Flexural strength of different curing conditions(Group SS30).

3.4. Analysis of microstructure and phase composition

As shown in Figure 4a, the intensity of the diffraction peak of the crystal increases gradually. In the XRD pattern of SS0 group without steel slag, there are glassy amorphous diffraction peaks, and the main reaction products are C-(N,K)-A-S-H gels and hydrotalcite. The hydration products in SS30 and SS70 groups are basically the same, which are mainly C-S-H gel and C-(N,K)-A-S-H gel, inert RO phase and $CaCO_3$ generated by carbonization. Despite 3d steam curing, the peak of the original mineral C_2S in steel slag still exists. As can be seen from Figure 4b, with the development of standard curing, the peak of C_2S gradually decreases and gel products increase. Later hydration may be dominated by C_2S, producing more C-S-H. This explains why the mechanical strength of the group mixed with steel slag in Figure 2a continued to increase in the later period. $Ca(OH)_2$ and AFt were not found in the XRD pattern, the reason was that the hydration reaction of steel slag and GGBFS promoted each other, leading to the consumption of $Ca(OH)_2$ in the slurry and the formation of C-S-H gel.

AAM-UHPC is mainly composed of hydration products generated by the reaction of steel slag powder and GGBFS powder interwoven to form a spatial network. The unhydrated powder and inert components in steel slag play a filling effect, and they are closely packed together to form a dense matrix.

Preprints (www.preprints.org) | NOT PEER-REVIEWED | Posted: 11 April 2023 doi:10.20944/preprints202304.0193.v1

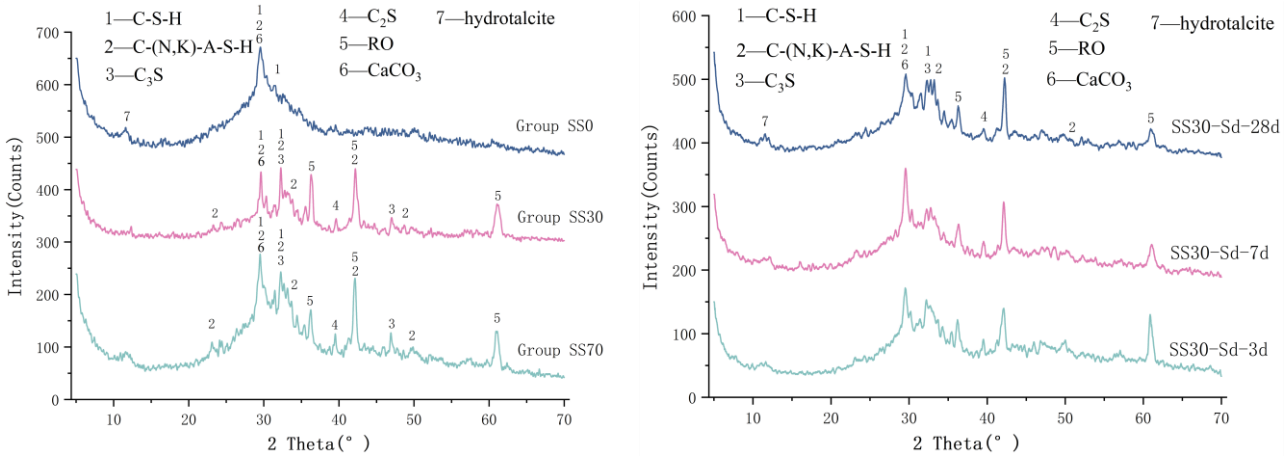

(**a**) (**b**)

Figure 4. XRD patterns of AAM-UHPC: (**a**) Different steel slag dosage; (**b**) Different curing conditions.

The SEM images at 3 d of steaming with different steel slag admixtures are shown in Figure 5. From Figure 5a, it can be observed that the matrix is flat, dense and smooth, with closed holes exposed due to crushing on the surface. The matrix in Figure 5b is more dense and almost no holes can be observed, and some unhydrated steel slag powder particles exist on the surface, which will continue to react with the alkaline material at a later stage. Due to the higher steel slag dosage, the matrix in Figure 5c is relatively more sparse, with the presence of clearly unhydrated fully hydrated steel slag particles hydrated in the middle of the picture. Amorphous C-S-H gels growing from the surface and near the steel slag particles, and cracks developing along weak interfaces near the steel slag particles during crushing.

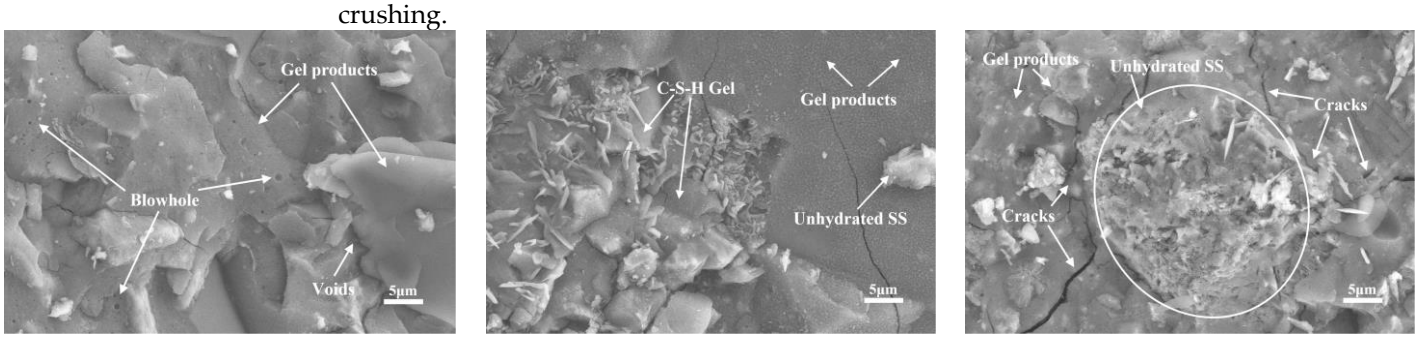

(**a**) (**b**) (c)

Figure 5. Microstructure of 3d AAM-UHPC with different dosage of steel slag: (**a**) Group SS0-3d; (**b**) Group SS30-3d; (c) Group SS70-3d.

Figure 6 shows the SEM images of the SS30 group at 3 d under different curing conditions. From Figure 6a, it can be found that C-S-H gels were formed in large quantities in the samples with standard curing, and some unhydrated GGBFS powder and steel slag powder particles, hexagonal sheet-like AFm-OH, and spherical silica fume in the center of the image were not fully reacted. In Figure 6b&c, it can be observed that the matrix is compact and flat under high temperature curing. The original amorphous C-S-H gel forms a monolithic plate, the unhydrated particles are smaller in size, and AFm-OH exists in the form of single crystals and fills the gaps between C-S-H and C-(N,K)-A-S-H gels, which not only improves the pore structure of the slurry, but also increases the density of the matrix, thus improving the early mechanical properties of AAM-UHPC.

Preprints (www.preprints.org) | NOT PEER-REVIEWED | Posted: 11 April 2023 doi:10.20944/preprints202304.0193.v1

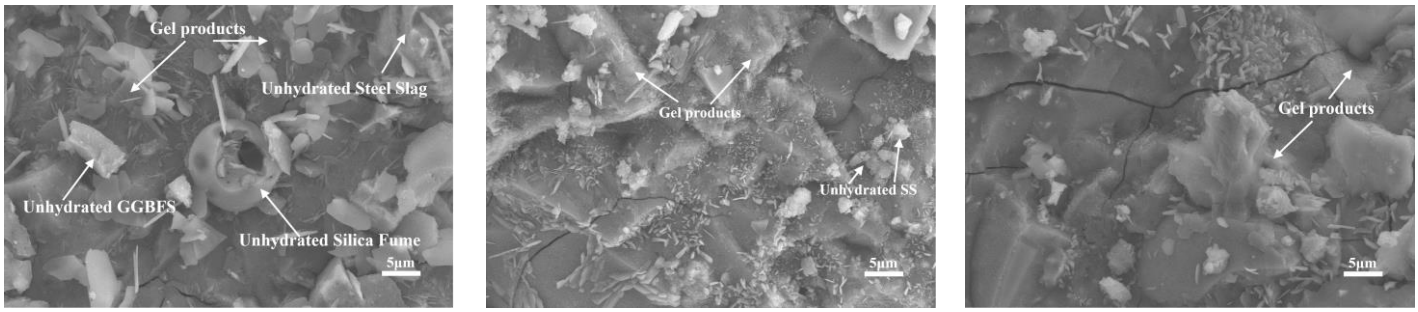

(**a**) (**b**) (c)

Figure 6. Microstructure of 3d AAM-UHPC under different curing conditions: (**a**) Group SS30-Sd(Standard)-3d; (**b**) Group SS30(steam)-3d; (c) Group SS30-HW(Hot Water)-3d.

3.5. Analusis of pore structure

The AAM-UHPC cured for 3 d was tested for pressures ranging from 0 to 60,000 psi, the porosity of SS0, SS30, and SS70 groups were 5.07%, 6.71%, and 4.98%, respectively, and the porosity of S30-St and S30-HW groups were 10.66% and 5.35%, respectively, the porosity and pore size distributions of each group are listed in Table 3.

As shown in Table 3, the average pore sizes of the SS0 and SS70 groups for 3 d of steam conditioning were 47.21 nm and 48.35 nm, but only 8.43 nm for SS30 group. Combined with their pore size distributions, it can be found that the pore size of SS30 group is mainly extremely fine gel pores.

The reasons for the excellent pore size distribution of SS30 group are as follows, on the one hand, compared with SS0 group, after mixing the correct amount of steel slag powder, it slows down the setting speed of the system, which can make the pores brought in during mixing discharge in time, and the particle size of steel slag powder can fill the particle size range of the break in mineral powder particle grading, thus improving the continuity of the overall gelling material grading; On the other hand, compared with SS70 group, the large mixing amount of steel slag hydration releases a large amount of Ca^{2+} is difficult to be absorbed by the GGBFS with less dosage [50], the continuous hydration of both is inhibited, which also leads to the reduction of the yield of the hydration product gel, and the increase of the matrix porosity especially the harmful void after hardening, leading to the reduction of the mechanical properties. While the particle stacking effect of SS30 group is more compact, and the hydration product fills the capillary pores between the powder particles, which also explains the source of its excellent mechanical properties.

Table 3. Different groups of AAM-UHPC porosity and pore size distribution

Group	Porosity/%	Average pore size/nm	Pore size distribution/%			
			<20 nm	20~100 nm	100~200 nm	>200 nm
SS0-3d	5.07	47.21	60.59	6.50	8.94	23.98
SS30-3d	6.71	8.43	38.08	4.95	7.43	49.22
SS70-3d	4.98	48.35	55.51	7.34	13.06	23.26
SS30-Sd-3d	10.66	14.93	52.41	11.41	7.54	28.62
SS30-Sd-7d	6.72	12.06	49.24	7.90	7.90	34.95
SS30-Sd-28d	6.01	19.43	50.17	15.67	8.71	25.08
SS30-HW-3d	5.35	10.21	53.66	5.02	2.70	37.83

As shown in Figure 7, the pore size of AAM-UHPC in all groups is dominated by harmless pores below 20 nm. From Figure 7a, it can be seen that the gel products continue to be generated as the curing progresses, the total porosity decreases, and the pore size distribution shifts toward smaller pore sizes, which also proves that there is a synergistic effect between steel slag powder and GGBFS powder [51], both the gel formed by GGBFS powder in the early reaction to provide the initial strength and the continued hydration

Preprints (www.preprints.org) | NOT PEER-REVIEWED | Posted: 11 April 2023 doi:10.20944/preprints202304.0193.v1

by steel slag powder to promote the densification of the structure and ensure the development of the later strength. From Figure 7b, it can be seen that the pore sizes of specimens under both steam and hot water curing conditions are dominated by harmless pores below 20 nm and less harmful pores from 20 to 100 nm, while the standard maintenance specimens are dominated by more harmful pores >200 nm, indicating that the high temperature curing at early ages is beneficial for the reaction of each solid waste component to proceed in an alkaline environment. The lower porosity is an important reason for AAM-UHPC to maintain better mechanical properties.

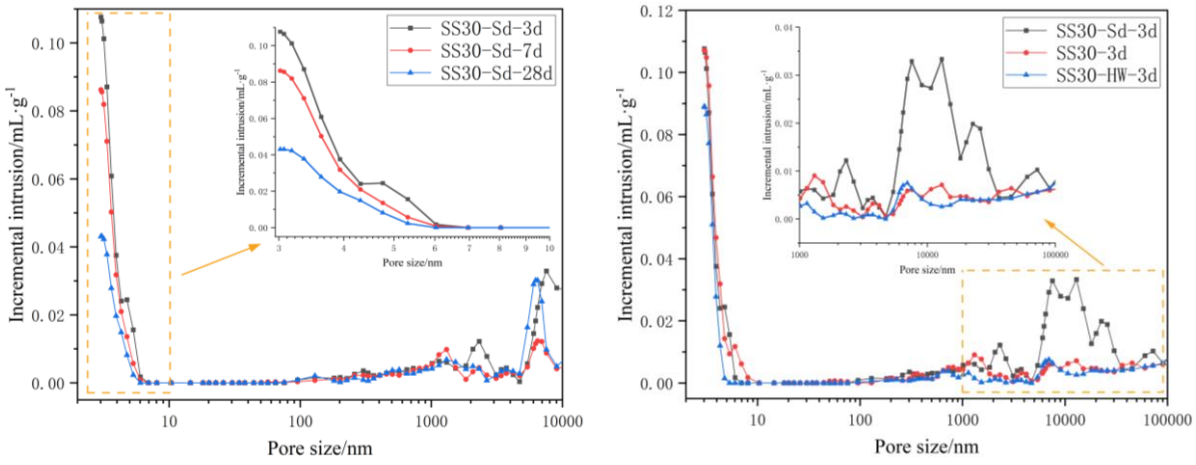

Figure 7. Pore size distribution of AAM-UHPC: (**a**) Different standard curing time; (**b**) Different curing conditions.

5. Conclusions

Blending with appropriate amount of steel slag powder can improve the comprehensive performance of AAM-UHPC, when the amount reaches 30%, UHPC matrix can produce the highest compressive strength of 156.1 MPa and the highest flexural strength of 16.32 MPa, at which time the it has both better working properties and mechanical properties.

Steel slag powder significantly improves the workability of AAM-UHPC, particular in terms of delaying the setting time and improving the flowability, thus making AAM-UHPC more suitable for engineering applications.

Steam or hot water curing at early age can promote the densification of the matrix structure, reduce porosity, and increase the volume of harmless pores, which is beneficial to strength development, but long-term hot and humid curing is detrimental, AAM-UHPC containing steel slag is suitable for early 3d steam curing combined with the subsequent standard curing.

The addition of steel slag changes the type of hydration products, which are mainly C-S-H and C-(N,K)-A-S-H gels, without $Ca(OH)_2$ besides RO phase and $CaCO_3$. GGBFS provides the early strength, steel slag ensures the later strength, and their synergistic effect promotes the development of the mechanical properties of AAM-UHPC.

The results of the present study indicate the need for further research aimed at the suitability of the matrix with fibers.

Author Contributions: Conceptualization, K.S. and H.D.; Methodology, K.S. and J.Z.; validation, K.S. and H.D.; Formal Analysis, K.S., H.D. and J.H.; Investigation, K.S. and H.D.; Data curation, K.S. and J.Z.; Writing—Review and Editing, K.S., H.D., J.H. and X.C.; Visualization, K.S.; Supervision, H.D.; Project Administration, Z.L.; Funding Acquisition, X.C. All authors have read and agreed to the published version of the manuscript.

Founding: This work was financially supported by the Natural Science Foundation of Hubei Province of China (2022CFB387) and the National Natural Science Foundation of China (No. 52178247) and (No.52179110).

Conflicts of Interest: The authors declare no conflict of interest.

References

1. Bache H H. COMPACT REINFORCED COMPOSITE BASIC PRINCIPLES.[J]. apr, 1987.
2. Larrard F D, Sedran T. Optimization of ultra-high-performance concrete by the use of a packing model[J]. Cement and Concrete Research, 1994, 24(6):997-1009.
3. Marvila M T, Azevedo A, Matos P , et al. Materials for Production of High and Ultra-High Performance Concrete: Review and Perspective of Possible Novel Materials.[J]. Materials, 2021(15).
4. Worrell E, Price L, Martin N. Carbon dioxide emissions from the global cement industry[J]. Annual Review of Energy and the Environment, 2001, 26:p.303-329.
5. Yu R, Spiesz P , Brouwers H. Development of an eco-friendly Ultra-High Performance Concrete (UHPC) with efficient cement and mineral admixtures uses[J]. Cement and Concrete Composites, 2015.
6. Abdulkareem O, Fraj A B, Bouasker M, et al. Mechanical and durabiliry properties of environmentally friendly Ultra-High-Performance Concrete (UHPC)[C]// The 3rd International Symposium on Ultra-High Performance Fiber-Reinforced Concrete (UHPFRC). 2017.
7. Li W, Huang Z, Zu T, et al. Influence of Nanolimestone on the Hydration, Mechanical Strength, and Autogenous Shrinkage of Ultrahigh-Performance Concrete[J]. Journal of Materials in Civil Engineering, 2016, 28(1):04015068.
8. Wang D, Shi C, Wu Z, et al. A review on ultra high performance concrete: Part II. Hydration, microstructure and properties[J]. Construction and Building Materials, 2015, 96:368-377.
9. Ministry of Environmental Protection, People's Republic of China Bulletin on the environmental condition of China in 2013.
10. Guo J, Bao Y, Min W. Steel slag in China: Treatment, recycling, and management[J]. Waste Management, 2018, 78(AUG.):318-330.
11. Yao, YonggangWang, WenlongGe, et al. Hydration study and characteristic analysis of a sulfoaluminate high-performance cementitious material made with industrial solid wastes[J]. Cement & concrete composites, 2020, 112(1).
12. Huang Y, Xu G, Cheng H, et al. An Overview of Utilization of Steel Slag[J]. Procedia Environmental Sciences, 2012, 16(none):791-801.
13. Qasrawi H, Shalabi F, Asi I. Use of low CaO unprocessed steel slag in concrete as fine aggregate[J]. Construction & Building Materials, 2009, 23(2):1118-1125.
14. A. Fernández-Jiménez a, B J G P, A F P. Alkali-activated slag mortars[J]. Cement and Concrete Research, 1999, 29(8):1313-1321.
15. Hailong, Radlinska, Aleksandra, et al. Understanding the drying shrinkage performance of alkali-activated slag mortars[J]. Cement & concrete composites, 2017.
16. Bakharev T. Geopolymeric materials prepared using Class F fly ash and elevated temperature curing[J]. Cement & Concrete Research, 2005, 35(6):1224-1232.
17. Temuujin J, Riessen A V, Mackenzie K. Preparation and characterisation of fly ash based geopolymer mortars[J]. Construction & Building Materials, 2010, 24(10):1906-1910.
18. Shi C, Day R L. Selectivity of Alkaline Activators for the Activation of Slags[J]. Cement Concrete and Aggregates, 1996, 18(1):8-14.
19. Somna K, Chai J, Kajitvichyanukul P, et al. NaOH-activated ground fly ash geopolymer cured at ambient temperature[J]. Fuel, 2011, 90(6):2118-2124.
20. Zerfu K, Ekaputri J J. Review on Alkali-Activated Fly Ash Based Geopolymer Concrete[J]. Materials Science Forum, 2016, 841:162-169.
21. Valente M, Sambucci M, Chougan M , et al. Reducing the emission of climate-altering substances in cementitious materials: A comparison between alkali-activated materials and Portland cement-based composites incorporating recycled tire rubber[J]. Journal of Cleaner Production, 2022, 333:130013-.
22. ZENG L, YU Y H, REN Y, et al. Preparation of Aerated Concrete with Alkali Activated Steel Slag and Blast Furnace Slag[J]. Journal of Building Materials, 2019, 22(02): 206-213（in Chinese）.
23. Wang X, Wang K, Li J , et al. Heavy metals migration during the preparation and hydration of an eco-friendly steel slag-based cementitious material[J]. Journal of cleaner production, 2021(Dec.20):329.
24. Randl N, Steiner T, Ofner S, et al. Development of UHPC mixtures from an ecological point of view[J]. Construction and Building Materials, 2014, 67:373-378.
25. Abdulkareem O M, Fraj A B, Bouasker M , et al. Microstructural investigation of slag-blended UHPC: The effects of slag content and chemical/thermal activation[J]. Construction and Building Materials, 2021(Jul.19):292.
26. Fan D, Yu R, Shui Z, et al. A new development of eco-friendly Ultra-High performance concrete (UHPC): Towards efficient steel slag application and multi-objective optimization[J]. Construction and Building Materials, 2021, 306:124913-.
27. Ahmed T, Elchalakani M, Karrech A, et al. ECO-UHPC with High-Volume Class-F Fly Ash: New Insight into Mechanical and Durability Properties[J]. Journal of Materials in Civil Engineering, 2021, 33(7):0003726.

28. Du J, Liu Z, Christodoulatos C , et al. Utilization of off-specification fly ash in preparing ultra-high-performance concrete (UHPC): Mixture design, characterization, and life-cycle assessment[J]. Resources, Conservation and Recycling, 2022, 180:106136-.
29. Chen W, Li B , Wang J , et al. Effects of alkali dosage and silicate modulus on autogenous shrinkage of alkali-activated slag cement paste[J]. Cement and Concrete Research, 2021, 141:106322.
30. Choi J I, Lee B Y, Ranade R, et al. Ultra-high-ductile behavior of a polyethylene fiber-reinforced alkali-activated slag-based composite[J]. Cement and Concrete Composites, 2016, 70: 153-158.
31. Cai R, Ye H. Clinkerless ultra-high strength concrete based on alkali-activated slag at high temperatures[J]. Cement and Concrete Research, 2021, 145: 106465.
32. Huang J Q, Zan H P, Yu Q J , et al. Effect of Setting Retarder on the Performance of Alkali-activated Carbonatite-slag Grouting Material[J]. Journal of Wuhan University of Technology, 2006, 28(4):20-23.
33. Bilim C, Karahan O, Atis C D , et al. Influence of admixtures on the properties of alkali-activated slag mortars subjected to different curing conditions[J]. Materials & Design, 2013, 44(FEB.):540-547.
34. Sasaki K, Kurumisawa K, Ibayashi K . Effect of retarders on flow and strength development of alkali-activated fly ash/blast furnace slag composite[J]. Construction and Building Materials, 2019, 216(AUG.20):337-346.
35. Su T, Zhou Y, Wang Q. Recent advances in chemical admixtures for improving the workability of alkali-activated slag-based material systems[J]. Construction and Building Materials, 2020, 272(9):121647.
36. "Research on set retarder of high and super high strength Alkali -activated slag cement and concrete." International Symposium on Ecological Environment and Technology of Concrete College of Materials Science and Engineering, Chongqing University, North street 83, Sapingba District, Chingqing, P. R. China, 400045;College of Materials Science and Engineering, Chongqing University, North street 83, Sapingba District, Chingqing, P. R. 2012.
37. Yang K, Basheer M, Yang C, et al. Site application of alkali-activated slag concrete in a Chinese building[J]. Concrete, 2021(9):55.
38. You N, Li B, Cao R, et al. The influence of steel slag and ferronickel slag on the properties of alkali-activated slag mortar[J]. Construction and Building Materials, 2019, 227(Dec.10):116614.1-116614.10.
39. Yu R, Spiesz P, Brouwers H J H. Mix design and properties assessment of ultra-high performance fibre reinforced concrete (UHPFRC)[J]. Cement and concrete research, 2014, 56: 29-39.
40. Sun J. Effect of silicate modulus of water glass on the hydration of alkali-activated converter steel slag[J]. Journal of thermal analysis and calorimetry, 2019, 138(1).
41. Wei Y, Cheng P, Ming Y, et al. Effects of Ultrafine and Highly Active Mineral Admixtures on Hydration and Shrinkage Properties of UHPC[J]. Bulletin of the Chinese Ceramic Society, 2022, 41(02): 461-468（in Chinese）.
42. Tang W J. Effect of Micro-powder Mixture of Steel Slag and Granulated Blast Furnace Slag on Cement and Concrete Properties[D]. China University of Geosciences, Beijing, 2009（in Chinese）.
43. Song W, Zhu Z, Peng Y, et al. Effect of steel slag on fresh, hardened and microstructural properties of high-calcium fly ash based geopolymers at standard curing condition[J]. Construction and Building Materials, 2019, 229: 116933.
44. Qiang W, Yan P, Mi G. Effect of blended steel slag–GBFS mineral admixture on hydration and strength of cement[J]. Construction and Building Materials, 2012, 35:8–14.
45. Sun X, Peng X, Zhang G, et al. Effect of steel slag content on properties of alkali-activated steel slag and slag based grouting material[J]. New Building Materials, 2017.
46. Mz A, Eh B. Effect of steel slag aggregate and bitumen emulsion types on the performance of microsurfacing mixture - ScienceDirect[J]. Journal of Traffic and Transportation Engineering (English Edition), 2020, 7(2):215-226.
47. Wang Q, Li M, Shi M. Hydration Properties of Cement-Steel Slag- Ground Granulated Blast Furnace Slag Complex Binder[J]. Journal of the Chinese Ceramic Society, 2014, 42(5).
48. Fang Y U, Xiong J B, Deng C L, et al. Study on the Influence of Curing Methods on Compressive Strength of C100 Ultra-high Strength Concrete[J]. Bulletin of the Chinese Ceramic Society, 2017.
49. Chi P, Zhang Y, Yang Y. Research on Mechanisim of Dry-wet heat Curing of Concrete[J]. Chinal Concrete & Cement Products, 2001.
50. Peng X Q, Liu C, Li S, et al. Research on the setting and hardening performance of alkali-activated steel slag-slag based cementitious materials[J]. Journal of Hunan University(Natural Sciences), 2015, 42(6):47-52.
51. Song W, Zhu Z, Pu S, et al. Efficient use of steel slag in alkali-activated fly ash-steel slag-ground granulated blast furnace slag ternary blends[J]. Construction and Building Materials, 2020, 259(1):119814.